Identification of cuproptosis-related subtypes, construction of a prognostic model, and characterization of the tumor immune microenvironment in gastric cancer

Dao Xin
The First Affiliated Hospital of Zhengzhou University
Yuxin Man
Sichuan Cancer Hospital, Medical School of University of Electronic Science and Technology of China
Yalan Yang
The First Affiliated Hospital of Zhengzhou University
Feng Wang (zzuwangfeng@zzu.edu.cn)
The First Affiliated Hospital of Zhengzhou University

Research Article

Keywords: copper, cuproptosis, prognostic model, cancer subtypes, stomach adenocarcinoma, tumor immune microenvironment

Posted Date: May 16th, 2022

DOI: https://doi.org/10.21203/rs.3.rs-1646621/v1

Abstract

Background: Gastric cancer represents a significant global public health burden worldwide. Although treatment strategies are continuously improving, the overall prognosis remains poor. Cuproptosis is a newly discovered form of cell death, and the relationship between cuproptosis in tumor immune microenvironment (TIME) and prognosis in STAD has hitherto not been reported.

Methods: Stomach adenocarcinoma (STAD) data were downloaded from TCGA and GEO databases. Bioinformatics analysis was performed to construct a cuproptosis-related risk model and identify cancer subtypes. The association between TIME and risk score was comprehensively explored.

Results: STAD samples were stratified into three subtypes according to prognostic cuproptosis gene expression. A cuproptosis risk model was constructed and validated based on the expression of 5 genes (*RPL39L, PEG10, SYNPO2, MMP11*, and *KRT17*). The model was significantly associated with the prognosis of STAD patients and TIME, including immune cell infiltration, microsatellite instability (MSI) status, tumor mutational burden (TMB) score, immune checkpoint, and human leukocyte antigen (HLA) gene expression. A prognostic nomogram based on the cuproptosis risk score was additionally constructed.

Conclusion: We identified a practical prognostic model based on cuproptosis-related genes in STAD and comprehensively established the relationship between cuproptosis and tumor immunity. Further research is warranted on the predictive value of the cuproptosis risk score during immunotherapy in gastric cancer patients in clinical practice and the molecular mechanisms by which cuproptosis influences the TIME.

1 Introduction

Gastric cancer (GC), including gastroesophageal junction (GEJ) adenocarcinoma, is the fourth leading cause of cancer-related mortality worldwide[1]. Stomach adenocarcinoma (STAD) is well-recognized as the most common pathological subtype. The majority of GC patients present with distant metastasis at the initial diagnosis. Treatment options for advanced GC have undergone significant evolution over recent years, developing from traditional chemotherapy to targeted therapy and immunotherapy, resulting in improved outcomes[2]. However, GC is a highly heterogeneous malignant tumor, and during clinical practice, many patients do not benefit from targeted therapy or immunotherapy[3]. Therefore, selecting the patient populations that potentially benefit from these treatments is critical for optimizing survival outcomes.

Copper is a mineral nutrient involved in cell proliferation and death pathways. It has long been thought that copper is only an active site metabolic cofactor. Emerging evidence suggests that copper is a dynamic signal metal and metal allosteric regulator [4]; for instance, copper-dependent phosphodiesterase 3B (*PDE3B*), mitogen-activated protein kinase kinase 1 (*MEK1*), and *MEK2* in cell growth and proliferation and the role of *ULK1* and *ULK2* in autophagy[5]. It remains unclear how excess copper induces cell death, warranting further studies. Cuproptosis is a new form of cell death recently

reported by Peter Tsvetkov et al.[6], distinct from documented death mechanisms, including apoptosis, pyroptosis, necroptosis, and ferroptosis. Researchers observed that cells highly dependent on mitochondrial respiration were more sensitive to cuproptosis, indicating a close association with the tricarboxylic acid (TCA) cycle. Several key genes have been associated with protein lipoylation. *FDX1* is an upstream regulator of protein lipoylation, and *FDX1* deletion inhibited *DLAT* lipoylation downstream. The present study provides the first evidence that copper promotes *DLAT* oligomerization and leads to increased levels of insoluble *DLAT*, leading to protein toxicity and cell death.

This study collected STAD samples from The Cancer Genome Atlas (TCGA) and Gene Expression Omnibus (GEO) databases for comprehensive analysis of cuproptosis-related gene (CRG) expression, mutation status, and copy number variations. Based on CRG expression patterns, all samples were classified into two cuproptosis-associated subtypes. According to differentially expressed gene (DEG) patterns between the two groups, samples were classified into three different gene subtypes. We successfully constructed a predictive model and comprehensively evaluated the correlations between different risk layers and the tumor immune microenvironment (TIME). To our knowledge, this is the first study to assess the relationships between cuproptosis, cancer immunity and prognosis in STAD patients. Our collective findings provide novel insights to aid in developing new strategies for accurate classification, effective immunotherapy, and innovative targeted therapy of gastric cancer.

2 Materials And Methods

2.1 Data collection

The RNA sequencing data and relevant clinical and follow-up information were obtained from TCGA and GEO (GSE84433) databases. FPKM values of TCGA-stomach adenocarcinoma (STAD) were converted and normalized to transcripts per kilobase million (TPM). We combined the two cohorts and excluded cases with missing follow-up information or unknown survival status. 745 STAD patients were included in this study for subsequent analysis. Clinical data such as TNM stage, pathological grade, age, gender, follow-up time, and survival status were collected. 10 cuproptosis genes were selected for analysis in this study (Table S1) according to a previously published study.

2.2 Somatic mutations and copy number alteration of CRGs

Somatic mutation statuses (workflow type: VarScan2 Variant Aggregation and Masking) and copy number variation (CNV) data were downloaded from TCGA database. The somatic mutation frequency in these 10 CRGs was summarized to select high mutation frequency cuproptosis genes. The somatic copy number alteration of CRGs was also analyzed. The correlation between CNV and mRNA expression and the location of these CRGs in the chromosomes were also identified.

2.3 Consensus clustering analysis of CRGs

The R package "ConsensusClusterPlus" was used for subsequent consensus unsupervised sample clustering analysis. STAD samples were divided into different subtypes based on CRG expression. To achieve an optimal subtyping effect, the cumulative distribution function (CDF) curve was increased gradually and smoothly, and the sample size was relatively balanced among the different subgroups.

2.4 Correlation of cuproptosis subtypes and clinicopathological characteristics and prognosis of STAD

We compared the relationships between molecular subtypes, clinicopathological characteristics, CRG expression, and prognosis to assess the clinical value of the two cuproptosis subtypes. Clinical factors included TNM stage, gender, age, and pathological grade. In addition, the differences in OS between the two subtypes were compared by the Kaplan–Meier curves.

2.5 Correlations of molecular subtypes with immune cell infiltrating and immune function

The Estimation of STromal and Immune cells in MAlignant Tumor tissues using Expression data (ESTIMATE) algorithm was used to evaluate each STAD patient's immune and stromal scores. The immune cell infiltration levels in STAD were determined using a single-sample gene set enrichment analysis (ssGSEA) algorithm. In addition, according to the ssGSEA results, immune function was simulated and calculated, including antigen-presenting cell inhibition or stimulation, immune checkpoint, human leukocyte antigen (HLA), T cell co-inhibition or co-stimulation, and type 1 or type 2 IFN-γ response.

2.6 DEGs identification and functional analysis

DEGs were selected between the different cuproptosis subgroups using the R package "limma" with a p-value<0.05 and a fold change of 1.5. Subsequent GSVA analysis was performed to identify the function and biological processes between different subgroups. GSVA was performed based on the hallmark gene set (c2.cp.kegg.v7.4.symbols.gmt) downloaded from MSigDB database. Functional enrichment analysis was also conducted using the R packages of "clusterProfiler" and "enrichplot" based on the DEGs.

2.7 Cuproptosis-related prognostic risk score

The cuproptosis-related prognostic risk score (CRG_score) was created to quantify the cuproptosis patterns of each STAD sample. DEGs associated with OS were selected according to univariate Cox regression. Next, all patients were divided into different cuproptosis gene clusters (A, B, C), followed by unsupervised clustering according to prognostic DEGs. All STAD (n=745) cases from TCGA and GEO

cohorts were combined and randomly divided into training (n=373) and validation cohorts (n=372) at a 1:1 ratio. The training cohort was used for subsequent analysis to construct the CRG_score. After univariate Cox regression analysis, Lasso regression was performed using the R package "glmnet". Multivariate Cox regression was eventually conducted to identify candidate prognostic cuproptosis genes. The CRG_score was calculated using the formula: CRG_score = Σ (Exp * coefi). Patients were further divided into high- and low-risk groups based on the median CRG_score.

Patients in the validation and all other cohorts were also divided into high- and low-risk groups using the same criteria. The distribution plot revealed a correlation between overall survival status and the CRG_score. Kaplan–Meier analysis was performed to compare the prognosis of the different risk groups in overall survival (OS) among the training, validation, and all cohorts. A heatmap was plotted to compare the differential expression patterns of prognostic CRGs between the two groups.

2.8 Immune landscape, microsatellite instability (MSI) status, cancer stem cell (CSC) index, tumor mutation burden (TMB) score, and HLA gene expression between high- and low-risk groups

The CIBERSORT algorithm was applied to explore the correlations of 22 infiltrating human immune cell types and CRG_score. The ESTIMATE algorithm assessed the immune and stromal scores between high- and low-risk groups. The correlation between the expression of 12 prognostic CRGs and immune cells were evaluated. We examined the associations between the CRG_score and immune checkpoint gene expression, MSI status, CSC index, TMB score, and HLA gene expression. A mutation annotation format (MAF) was performed to compare STAD patients in high- and low-risk groups using the maftools R package.

2.9 Drug susceptibility analysis

To explore the application value of CRG_score in clinical drug selection, the R package "pRRophetic" was used to assess the drug susceptibility in the two risk groups and calculate the semi-inhibitory concentration (IC_{50}) values for commonly used chemotherapy or targeted therapeutic drugs.

2.10 Construction and validation of a CRGs related nomogram

Univariate and multivariate Cox regression analyses were performed to select potential independent prognostic factors. A prognostic nomogram was constructed by integrating the CRG risk score with common clinical variables. We additionally generated calibration curves for 1-, 3-, and 5-year OS to

compare the model prediction performance with actual outcomes. Decision curve analysis (DCA) analysis was conducted to estimate the predictive value of the nomogram on clinical decision-making.

2.11 Human Tissues and Quantitative Real Time-Polymerase Chain Reaction

We obtained 14 cancer and their paired normal tissues from gastric cancer patients who underwent stomach surgery in the First Affiliated Hospital of Zhengzhou University. The study was performed in line with the principles of the Declaration of Helsinki and approved by the First Affiliated Hospital of Zhengzhou University Research Ethics Committee. Written informed consent was provided by each patient. Total RNA was extracted by Trizol reagent (Takara, Beijing, China) according to the manufacturer's protocol. The synthesis of cDNAs corresponding to the mRNAs of interest was conducted using the PrimeScript RT reagent Kit with gDNA Eraser (Takara) and SYBR Green Premix (Cowin Biosciences, Jiangsu province, China) with specific PCR primers (Sangon Biotech Co., Ltd, Shanghai, China). The data were normalized to GAPDH.

2.12 Statistical analysis

Statistical analysis in this study was performed using R software version 4.1.1. The Student's t-test or Wilcoxon test was used for the difference between the two groups, and ANOVA was used to compare more than two groups. Statistical significance was set at a p-value<0.05.

3 Results

3.1 Mutation landscape and copy number alteration of CRGs in STAD

The flowchart of the whole study is presented in Fig. 1. A total of 10 cuproptosis genes were included in this study. Mutational analysis showed that cuproptosis genes had a relatively high mutation frequency in STAD. Among the 433 STAD samples, 56 (12.93%) had cuproptosis gene mutation (Fig. 2a). 8 (80%) genes had different mutation frequencies and types. The highest mutation frequency gene was *CDKN2A* (4%), followed by *DLAT* (3%), *DLD, MTF1, LIPT1* (2%), and *GLS, LIAS, PDHB* (1%). We did not observe *FDX1* and *PDHA1* mutations in STAD samples. We searched the Cbioportal database and recorded each gene's most common mutation sites. The M274V mutation was observed in the second exon of *PDHB* (Fig. 2b), while *FDX1* harbors the G151D mutation in the fourth exon (Fig. 2c). Fig S1 presents the common mutation site of other cuproptosis genes.

Next, we assessed the copy number variation (CNV) of the cuproptosis genes and found that they all had different CNV frequencies. *GLS, MTF1*, and *LIPT1* were associated with an increased CNV, while the CNV

was decreased for *CDKN2A, DLAT, FDX1, PDHB*, and *DLD* (Fig. 2d). 10 cuproptosis genes were located in the different sites of 23 chromosomes, and it showed that *MTF1* was located in the first chromosome, *LIPT1* and were located in the second chromosome, and other genes were located in the different chromosomes, respectively (Fig. 2e). We also explored cuproptosis gene expression differences between STAD and normal samples. Nine genes were differentially expressed, and all exhibited significantly higher STAD expression than normal samples. Cuproptosis genes with CNV gain, such as *GLS, MTF1*, and *LIPT1*, were significantly elevated in STAD samples, indicating that CNV might regulate mRNA expression of cuproptosis genes. In contrast, genes with CNV loss, such as *DLD, PDHA1, CDKN2A, DLAT, FDX1*, and *PDHB*, exhibited upregulated mRNA expression, while other genes with high frequencies of CNV gain or loss showed no differences between tumor and normal samples, such as *LIAS*, suggesting that CNV is not the only factor influencing the expression of cuproptosis genes. Indeed, other factors, including non-coding RNA, DNA methylation, m6A RNA methylation, and transcription factors, could also regulate cuproptosis gene expression.

3.2 Identification of cuproptosis subtypes in STAD

Univariate Cox regression analysis revealed the prognostic significance of 10 cuproptosis genes in STAD patients (Table S2). Based on the univariate Cox regression analysis, a prognostic cuproptosis network was established, which showed the comprehensive landscape, interrelationships between each cuproptosis gene, and their predictive value in STAD (Fig. 2f). Five cuproptosis genes showed OS-related significance, including *FDX1, LIAS, LIPT1, DLAT*, and *PDHA1*. Kaplan-Meier curves showed that STAD patients with high expression of the 5 genes had a longer OS than those with a lower expression (Fig. 2g, 2h, S2). Furthermore, most cuproptosis genes were expressed differentially between STAD and normal samples (Fig. 2i).

According to the expression of CRGs, we divided STAD patients into different clusters using a consensus clustering algorithm (**Fig S3**). k = 2 was the appropriate choice for dividing the patients into subtypes A (n = 531) and B (n = 245) (Fig. 3a, **Table S3**). At k = 2, the sample size was relatively balanced between the two subgroups. PCA analysis showed a significant difference in cuproptosis transcription profile between subtypes A and B (Fig. 3b), while the Kaplan Meier curves showed no difference in OS between subtypes A and B (p = 0.487; Fig S4). Further analysis revealed relative differences in cuproptosis gene expression and clinical features between the two subgroups (Fig. 3c).

3.3 Function analysis and TME characteristics in distinct cuproptosis subtypes

To compare functional differences between the two cuproptosis subgroups, we performed GSVA analysis and found that subtype B was significantly enriched in steroid biosynthesis and cell cycle-related pathway, while subtype A was mainly enriched in cell apoptosis and immune-related pathways, including

NK cell-mediated cytotoxicity, T cell receptor pathway, B cell receptor pathway, leukocyte transendothelial migration, and chemokine signaling pathway (Fig. 4a, **Table S4**).

According to the ssGSEA results, we calculated the immune cell infiltration in each STAD sample and observed significant differences in the infiltration of most immune cells between the two cuproptosis subtypes (Fig. 4b). The infiltrating levels of B cell, CD8 + T cell, dendritic cell, Macrophages, mast cells, neutrophils, NK cell, naive T cell (Tfh cell), T helper 1 cell, and T helper 2 cells were significantly higher in subtype A than subtype B. This result was consistent with the GSVA enrichment analysis. Several kinds of immune functions such as APC co-stimulation, immune checkpoint function, cytolytic activity, Chemokines, and Chemokine Receptors (CCR), HLA function, inflammation-promoting function, T cell inhibition, T cell stimulation, and type 2 IFN-γ response exhibited higher enrichment levels in subtype A than in subtype B (Fig. 4c). In addition, we assessed the TME score, including the stromal score, immune score, and estimate score of the two cuproptosis subtypes using the ESTIMATE package. A higher stromal or immune score suggested a higher infiltration and activity of stromal cells and immunity (Fig. 4d). Overall, subtype A was associated with a higher immune and stromal score.

3.4 Cuproptosis gene cluster based on prognostic DEGs

We identified 103 cuproptosis-related DEGs between A and B subtypes using the R package "limma" (Table S5). Functional analysis was performed based on these DEGs. First, GO analysis revealed that DEGs were significantly enriched in biological processes associated with the metabolism of intracellular substances, including metabolism and olefinic compound metabolic process. They were also enriched in molecular functions, such as endopeptidase activity (Fig. 5a).

Then, a univariate Cox regression analysis was performed, and 26 prognostic DEGs related to OS for STAD were identified ($p < 0.05$, **Table S6**). A new consensus clustering was conducted to evaluate potential regulation mechanisms based on these prognostic DEGs; STAD patients were divided into three cuproptosis gene subtypes, gene subtype_A, gene subtype_B, and gene subtype_C ($k = 3$, Fig. 5b, S5, **Table S7**). Significant differences were observed in six CRG expressions between three gene clusters, including *FDX1*, *LIAS*, *LIPT1*, *DLAT*, *PDHA1*, and *CDKN2A* (Fig. 5c). Figure 5d shows the relative differences in T, N classification, age, gender, TNM stage, pathological grade, and cuproptosis cluster between gene subtypes A, B, and C. The ESTIMATE analysis showed that clusters A, B, and C had significantly different TME scores, and subtype C had the highest stromal score and a relatively higher immune score (Fig. 5e). In addition, the Kaplan-Meier curve showed that gene subtype A had the best OS, while subtype_C had the shortest median OS ($p < 0.001$, Fig. 5f).

3.5 Construction and validation of the prognostic cuproptosis risk score

STAD patients from TCGA and GEO cohorts were combined and randomly divided into training and validation cohorts at a ratio of 1:1. The training cohort was used for the next analysis. LASSO analysis was performed for 26 prognostic DEGs, and 9 genes were selected for subsequent multivariate Cox regression analysis (Fig. 6a, b). Finally, we obtained 5 prognostic CRGs that were high-risk genes, including *RPL39L, PEG10, SYNPO2, MMP11*, and *KRT17*(**Table S8**). Based on the multivariate Cox regression analysis results, the CRG risk score was calculated as follows: CRG risk score = (0.1098 * expression of *RPL39L*) + (0.1460 * expression of *PEG10*) + (0.1657* expression of *SYNPO2*) + (0.1701* expression of *MMP11*) +(0.0598* expression of *KRT17*). Based on the median CRG risk score, all STAD patients were divided into high- and low-risk groups.

The CRG risk_score was significantly different among the two cuproptosis and three gene clusters (Fig. 6c, d). The CRG score was lowest in gene cluster_A; no significant differences were observed between B and C (p = 0.89), consistent with the Kaplan-Meier analysis findings. The Sankey plot allowed visualization of the interrelationships among two cuproptosis clusters, three gene clusters, risk_score, and overall survival status (Fig. 6e). The distribution plot showed that the OS of STAD decreased with increased CRG risk_score (Fig. 6f, g). The correlation results in the whole-patient and validation set are presented in **Fig S6**. Kaplan–Meier curve analysis showed significantly longer OS in the low-risk relative to the high-risk group ($p < 0.001$, Fig. 6h). ROC curves indicated that the CRG risk_score had potential value in predicting OS of STAD patients at 1, 3, and 5 years, with AUC values of 0.645, 0.698, and 0.704, respectively (Fig. 6i). We obtained similar results in the whole-patient and validation set **(Fig S7**). In addition, the majority of cuproptosis-related genes were differentially expressed between the two risk groups, including *LIAS, DLAT, PDHA1, PDHB, CDKN2A*, and *FDX1* **(**Fig. 6j). In the training cohort, a heatmap was generated to establish the relationships of the 5 prognostic marker genes with CRG risk groups. All 5 genes were highly expressed in the high-risk group (Fig. 6k).

3.6 Validation of the expression of the 5 prognostic cuproptosis genes in the prognostic model

The expression levels of 5 prognostic genes were measured in 14 pairs of STAD tissues and normal adjacent tissues by RT-qPCR. As shown in **Fig S8**, *KRT17*, *MMP11*, and *RPL39L* exhibited significantly higher expression in STAD tissue than normal tissue. *SYNPO2* was lower in the STAD tissue with no significant difference between the expression of *PEG10* in STAD and corresponding normal tissues. Results of RT-qPCR are presented in **Table S9**. According to the HPA database, expression levels of *KRT17* were higher in STAD than in normal tissues, suggesting this gene may be a risk factor. Moreover, *RPL39L* and *SYNPO2* exhibited lower expression levels in STAD than in normal tissues, suggesting that these genes are protective factors. There was no significant difference between the expression of *MMP11* and *PEG10* (Fig. 7). The primers used in PCR assays are listed in **Table S10**.

3.7 Tumor microenvironment evaluation in the high- and low-risk groups

The CIBERSORT algorithm results revealed positive associations between the prognostic CRG risk_score with resting CD4 T memory cells, activated NK cells, resting mast cells, M0 macrophages, and M2 macrophages, and negative correlations with activated memory CD4 T cells, $CD8^{+}$T cells, follicular helper T cells, resting NK cells, resting dendritic cells, and M1 macrophages (Fig. 8a, **Table S11**).

The ESTIMATE algorithm was additionally applied to simulate TIME. The results showed that a high CRG risk_score was associated with a high stromal score in STAD samples, while the immune score was not significantly different between high and low-risk groups (Fig. 8b, **Table S12**).

The relationship between 5 prognostic cuproptosis genes and 22 human immune-related cells was further examined (Fig. 8c**).** Most immune cells were significantly positively or negatively regulated by the 5 genes. Importantly, the *SYNPO2* gene was positively correlated with resting memory CD4 T cells, activated NK cells, resting mast cells, M2 macrophages, and memory B cells and negatively with follicular helper T cells, activated memory CD4 T cells, resting NK cells, M1 macrophages, and resting dendritic cells, suggesting that *SYNPO2* might play a vital role in the regulatory role of cuproptosis in TIME. In addition, the relationship between CRG prognostic risk_score and immune checkpoints was further assessed (Fig. 8d). 9 immune checkpoints were differentially expressed in the different cuproptosis risk groups, including *TNFSF4, ICOS, VTCN1, CD44, NRP1, CD160, LGALS9, KIR3DL1*, and *CD276*.

3.8 Correlations of CRG risk_score with MSI, CSC index, HLA gene expression, and TMB score

Experiments were performed to determine the relationship between the CRG risk_score with immunotherapeutic biomarkers, such as MSI, CSC index, HLA gene expression, and TMB score. We first analyzed the distribution of somatic mutations between the two cuproptosis risk groups in the TCGA STAD cohort. Low-risk samples showed relatively higher mutation frequency than the high-risk group (90.57% vs. 83.67%, Fig. 9a,b). Multiple genes displayed distinct mutation types and frequencies in gastric cancer cells. For example, the frequency of *TTN* mutation was 44% in the high-risk group and 49% in the low-risk group. The top 5 mutated genes in the high- and low-risk groups were *TTN, TP53, MUC16, ARID1A*, and *LRP1B*. Besides, the TMB score was negatively associated with the cuproptosis gene cluster in this study (**Fig S9**) and significantly lower in the high-risk group than the low-risk group (Fig. 9c). The CRG risk_score showed a negative linear correlation with the CSC index (R= -0.57, $p < 0.001$, Fig. 9d), indicating that STAD cells with high CRG risk_score have less distinct stem cell properties and a higher level of cell differentiation. Notably, a low CRG risk_score was significantly correlated with the MSI-H status. The MSI-H status in the low-risk group was higher than in the high-risk group (20% vs. 12%)(Fig. 9e), and the median risk_score of MSI-H was relatively lower than for MSI-L ($p = 0.079$) and MSS groups ($p = 0.012$; Fig. 9f). We additionally performed a correlation analysis between CRG risk_score and HLA

gene expression. Our results showed lower expression of *HLA-DMA* and *HLA-F* in the high-risk group relative to the low-risk group (Fig. 9g).

3.9 Drug susceptibility analysis

We performed drug susceptibility analysis to select promising chemotherapy or targeted drugs for high- and low-risk groups of STAD. Interestingly, patients in the high-risk group had lower IC_{50} values for docetaxel, lapatinib, pazopanib, and imatinib, while those in the low-risk group had significantly lower IC_{50} values for sorafenib (Fig. 9h-l). These results corroborate the value of the cuproptosis risk score in predicting drug sensitivity and selection of potential beneficiaries of specific treatment chemotherapy and targeted therapy drugs among STAD patients.

3.10 Construction and validation of nomogram based on CRG risk_score

Univariate and multivariate Cox regression analyses were performed, and factors, including age, T, N, M classification, and the cuproptosis risk score, were independent prognostic factors in this study (Fig. 10a,b). A nomogram was constructed by incorporating the cuproptosis risk_score and common clinicopathological factors to predict OS at 1, 3, and 5 years (Fig. 10c). The C-index of the model was 0.746, indicating a relatively good prognostic value of the nomogram. The calibration curves of the nomogram indicated excellent consistency with the standard curve between predicted and actual 1-,3-, and 5-year OS rates in STAD patients (Fig. 10d). DCA was conducted to evaluate the predictive value of the nomogram in clinical decision-making (Fig. 10e). Notably, the nomogram showed better reliability than the TNM stage.

4 Discussion

Apoptosis is a common pathway of programmed cell death in the body. It is well-established that traditional chemotherapeutic drugs mainly exert their effects by promoting apoptosis of tumor cells, with resistance to apoptosis established as the predominant mechanism underlying tumor drug resistance[7]. In recent years, the comprehensive investigation of the pathways of tumor cell apoptosis has led to the gradual discovery of novel programmed cell death modes, such as pyroptosis, ferroptosis, and necroptosis. Most importantly, cuproptosis is the latest reported form of programmed cell death.

Metals are an essential part of all life forms required for almost all enzyme functions and are closely related to almost all basic biological processes. Metals have three main functions: providing structural support, acting as enzymes cofactor, and mediating electron transport. In addition, researchers found that metals are closely related to cancer development and tumor immune function[8, 9].

Ferroptosis is a new type of cell death form discovered in recent years, usually accompanied by a large amount of iron accumulation and lipid peroxidation[10, 11]. Ferroptosis inducers can directly or indirectly affect glutathione peroxidase through different pathways, resulting in decreased antioxidant capacity of cells, accumulation of lipid reactive oxygen species (ROS), and ultimately oxidative death of cells[12]. Similarly, copper can mediate cell death through cytotoxicity induced by increased mitochondria-dependent energy metabolism and ROS accumulation in a process called cuproptosis. Before the concept of cuproptosis was established, researchers demonstrated the value of copper in the occurrence and development of cancer.

Similar to iron, copper is a mineral nutrient increasingly reported to be involved in cell proliferation and death pathways. Copper's inherent oxidation-reduction (redox) property accounts for its benefits and potential toxicity to cells. Copper is an essential cofactor of enzymes that mediate many essential cell functions, but dysregulation of intracellular copper storage can cause oxidative stress and cytotoxicity. An increasing body of evidence suggests that cancer progression is associated with increased intracellular copper concentration, and tumor cells require more copper than normal cells. Copper is also involved in cell proliferation, angiogenesis, cancer metastasis, epithelial-mesenchymal transition, and the formation of the tumor microenvironment [13, 14]. The *ATP7A–LOX* pathway has been reported to promote tumor growth and metastasis in breast and lung carcinoma cell lines and mice models by regulating intracellular copper delivery[15].

New evidence suggests that copper is a dynamic signaling metal and allosteric regulator that regulates and coordinates biological activity in response to external stimuli. Copper is required for the activity of the autophagic kinases *ULK1* and *ULK2* (*ULK1/2*) through direct copper-*ULK1/2* interaction. Genetic loss of mutations in copper transporters CTR1 or *ULK1* mutation disrupts binding of copper reduced *ULK1/2*-dependent signaling and the formation of autophagosome complexes and diminishes growth and survival of lung carcinoma driven by $KRAS^{G12D}$ [16]. The *RAS/RAF/MEK/ERK (MAPK)* signaling cascades are critical for intercellular and intracellular communication and regulate basic cell functions such as growth, survival, and differentiation. Copper has been associated with the intracellular level of *ERK1/2* phosphorylation in response to proliferative signals in melanoma cell lines. Copper-treated cancer cells were found to exhibit increased activation levels of receptor tyrosine kinases *TRKB*, *EGFR*, and upstream of *MAPK* signaling [17, 18]. Importantly, copper metallization promotes protein degradation through allosteric activation of the E2 binding enzyme *UBE2D1-UBE2D4*. As a result, many proteins are labeled and degraded by ubiquitin, especially p53. Thus, an excessive supply of copper in malignant tumor cells leads to a diminution of p53, which may play a role in tumor cells' inability to undergo programmed cell death [19].

Mechanisms of cuproptosis first illustrated by Tsvetkov et al. suggested that excess intracellular copper could induce the aggregation of lipoylated dihydrolipoamide S-acetyltransferase (*DLAT*), which is associated with the mitochondrial TCA cycle, resulting in proteotoxic stress and leading to a novel form of cell death [20]. Cuproptosis is distinct from apoptosis because it does not involve either the cleavage or activation of caspase 3 activity, the hallmark of apoptosis. In addition, after cells were treated with

elesclomol, a kind of copper ionophore, the killing potential was maintained when the key effectors of apoptosis, BAX, and BAK1, were knocked out. It was also found that cuproptosis was not abrogated when cells were treated with inhibitors of necroptosis, ferroptosis, and oxidative stress, suggesting that cuproptosis is distinct from currently known programmed cell death modes [6, 20].

To the best of our knowledge, there is currently no report on the predictive value of cuproptosis-related genes in tumor prognosis and tumor immune environment. This study investigated the genetic features and transcriptional alterations in cuproptosis-related genes in STAD. Based on CRG expression, STAD samples were divided into two clusters (A and B) and differences in OS were not significant. The functional enrichment analysis revealed enrichment of several immune activation-related signals in cluster B, including steroid biosynthesis, NK cell-mediated cytotoxicity, T cell receptor pathway, B cell receptor pathway, leukocyte transendothelial migration, and chemokine signaling pathway. We further identified 103 cuproptosis-related DEGs between subtypes A and B, among which 26 were associated with OS in STAD patients. According to the 26 prognostic DEGs, patients were divided into three cuproptosis gene clusters (gene subtypes A, B, and C). The gene cluster system was highly associated with the OS of STAD patients, and most CRGs were differentially expressed among the three gene clusters. The results collectively support the potential of CRGs as prognostic and immunotherapeutic biomarkers.

Next, we constructed and validated a useful prognostic model based on the CRG risk_score and patients were eventually classified into high- and low-risk groups. Patients in the low-risk group had significantly better OS than those in the high-risk group. We subsequently explored the tumor immune microenvironment between the high- and low-risk groups. Several human immune cells were correlated with CRG risk_score, including resting memory CD4 T cells, activated NK cells, resting mast cells, M0 macrophages, M2 macrophages, activated memory CD4 T cells, $CD8^{+}$T cells, follicular helper T cells, resting NK cells, resting dendritic cells, and M1 macrophages. Significant differences in the stromal score, MSI status, TMB score, CSC index, HLA gene expression, and immune checkpoint expression levels were observed between high- and low-risk groups. Importantly, drug susceptibility analysis may be used in clinical practice to select potentially effective drugs for STAD based on cuproptosis gene expression. In the present study, a hitherto undocumented prognostic nomogram based on cuproptosis-related genes in STAD patients was established, and its predictive ability was validated.

Current treatments for gastric cancer include resection of the tumor via gastroscopy or surgery, chemotherapy, targeted therapy, and radiotherapy. Despite considerable progress in developing treatment strategies for gastric cancer, therapeutic outcomes remain unsatisfactory. Immunotherapy is an effective strategy for various tumor types, including gastric cancer, due to its precise effects on the tumor microenvironment and persistent response[2, 21]. While immunotherapy offers new hope, many patients do not benefit from this mode of treatment, mainly due to tumor heterogeneity and complex tumor immune microenvironments, which should be a focus of further research[22]. The TIME is widely acknowledged for its extreme complexity, including surrounding blood vessels, immune cells, fibroblasts, bone marrow-derived inflammatory cells, various signaling molecules, and an extracellular matrix. The

tumor microenvironment has been shown to play an essential role in malignant progression, immune escape, and immunotherapy resistance by altering the ratio of immunosuppressive and cytotoxic responses in the vicinity of the tumor.

In addition to being an essential nutrient and signal regulator, metal is also involved in regulating immune responses, including antitumor immunity [23]. Previous studies have also reported the corresponding value of copper in the tumor immune microenvironment. Florida Voli et al. found a strong correlation between the major copper influx transporter copper transporter 1 (CTR-1) and PD-L1 expression across many cancers but not in corresponding normal tissues and substantiated that copper supplementation enhanced PD-L1 expression at mRNA and protein levels in cancer cells via EGFR and STAT signaling pathways, mediating PD-L1 driven cancer immune evasion in mice models [24]. Overwhelming evidence substantiates that mast cells participate actively in various other diseases, such as arthritis, cancer, and bacterial infection, and copper can regulate mast cell maturation by mediating MAPK signaling[25]. However, no report has illustrated the function of cuproptosis in TIME so far. Importantly, this is the first study to assess the correlation between cuproptosis and cancer immunity.

Tumor-associated macrophages (TAMs), the major component of myeloid cells in tumors, exhibit two major phenotypes: M1 (inhibiting cancer progression) and M2 (promoting cancer progression) macrophages[26]. TAMs exert both pro-tumor and antitumor effects and may serve as attractive potential targets for tumor therapy. Zhao et al. reported that TAMs isolated from gastric cancer tissues predominantly display an M2 phenotype, and gastric cancer-derived mesenchymal stromal cells promote metastasis and epithelial-mesenchymal transition (EMT) by triggering M2 TAM polarization through the IL-6/IL-8-JAK2-STAT3 signaling pathway[27]. Moreover, blockage of M2 TAMs could reactivate CD8 + T cells against immunosuppressive tumors, and the infiltration levels of M2 TAMs in gastric cancer were associated with the 5-year survival rate[28, 29]. Herein, we observed increased infiltration of M2 TAMs in the high cuproptosis risk_score group, suggesting that cuproptosis may participate in the antitumor immune response via regulation of macrophages. However, further research is warranted to establish precise molecular mechanisms.

Immunotherapy has become an indispensable element of gastric cancer treatment. ICIs represent a critical aspect of immunotherapy, including anti-PD1 and anti-CTLA4 antibodies, which have continuously improved the survival of gastric cancer patients and progressed from back-line to front-line status in clinical practice. Several researchers have focused on the selection of effective immunotherapy biomarkers to date. MSI-H/dMMR is generally recognized as an excellent predictive biomarker in gastrointestinal tumors. In previous studies, MSI-H accounted for 19.09% of STAD cases in a TCGA cohort and 5.75% cases in a Chinese cohort, which were higher relative to the proportion of MSI-H in other solid tumor types[30]. Moreover, the KEYNOTE-061 and KEYNOTE-062 clinical trials reported higher OS, progression-free survival (PFS), and objective response rate (ORR) with anti-PD1 therapy than chemotherapy for MSI-H gastric cancer patients[31, 32]. In the present investigation, MSI-H patients accounted for a higher percentage of the low-risk group than the high-risk group, and the median risk_score of MSI-H was markedly lower than the MSI-L/MSS groups. The majority of immune checkpoint

genes were differentially expressed between the high- and low-risk cuproptosis groups, confirming the value of exploring cuproptosis in new immunotherapy approaches targeting other checkpoints. The tumor cell-killing function of immune cells reportedly depends on efficient antigen presentation by human leukocyte antigen (HLA) molecules. Accumulating evidence suggests that HLA serves as a useful predictor of the efficacy of immunotherapy, and HLA typing before treatment is an informative step for therapy[33]. In our experiments, HLA-DMA and HLA-F displayed distinct expression patterns among different cuproptosis risk groups, supporting their potential utility in predicting response to ICB and designing neoantigen-based therapeutic vaccines in the future. We conclude that a high cuproptosis risk_score is correlated with low MSI-H percentage, low expression of immune checkpoints, low TMB score, and effector immune cells in STAD. Indeed, precision therapy relies on accurate typing and a comprehensive understanding of the underlying mechanisms. Given that cuproptosis is a biological process with a central role in developing gastric cancer and regulation of TIME, exploration of the efficacy of targeted cuproptosis therapy alone or in combination with immunotherapy should be the focus of future studies.

In conclusion, we identified a practical prognostic model based on cuproptosis-related genes in STAD and comprehensively analyzed the relationship between cuproptosis and tumor immunity-associated factors. Our results provide the foothold for exploring novel and innovative targeted and immunotherapy approaches for STAD. In our future studies, the predictive value of cuproptosis risk_score will be assessed in immunotherapy for gastric cancer in clinical practice to establish the molecular pathways by which cuproptosis influences the immune microenvironment.

Declarations

Conflict of Interest

The authors declare that the research was conducted in the absence of any commercial or financial relationships, and there is no conflict of interest.

Author Contributions

DX, YXM, and YLY wrote the manuscript and performed bioinformatics analysis. DX, FW contributed to the manuscript discussion. DX and FW designed the study, and YXM researched the literature and contributed to figures and tables. FW supervised the study and contributed to data analysis. All authors read and approved the final manuscript.

Funding

This work was supported by Henan Provincial Science and Technology Research Project (No. SBGJ202002080), Leading Talent Training in Henan Province (No. YXKC2020017).

Acknowledgments

None.

Data Availability Statement

The datasets presented in this study can be found in online repositories and supplementary material. Additional data and the code used to analyze the data can be requested by mail to the corresponding author.

References

1. Sung H, et al.(2021). Global Cancer Statistics 2020: GLOBOCAN Estimates of Incidence and Mortality Worldwide for 36 Cancers in 185 Countries. CA: a cancer journal for clinicians;71(3):209-49.http://dx.doi.org/10.3322/caac.21660
2. Joshi SS, et al.(2021). Current treatment and recent progress in gastric cancer. CA: a cancer journal for clinicians;71(3):264-79.http://dx.doi.org/10.3322/caac.21657
3. Seeneevassen L, et al.(2021). Gastric Cancer: Advances in Carcinogenesis Research and New Therapeutic Strategies. International journal of molecular sciences;22(7).http://dx.doi.org/10.3390/ijms22073418
4. Gupte A, et al.(2009). Elevated copper and oxidative stress in cancer cells as a target for cancer treatment. Cancer treatment reviews;35(1):32-46.http://dx.doi.org/10.1016/j.ctrv.2008.07.004
5. Ge EJ, et al.(2022). Connecting copper and cancer: from transition metal signalling to metalloplasia. Nature reviews Cancer;22(2):102-13.http://dx.doi.org/10.1038/s41568-021-00417-2
6. Tsvetkov P, et al.(2022). Copper induces cell death by targeting lipoylated TCA cycle proteins. Science (New York, NY);375(6586):1254-61.http://dx.doi.org/10.1126/science.abf0529
7. Fernández A, et al.(2015). Melatonin and endoplasmic reticulum stress: relation to autophagy and apoptosis. Journal of pineal research;59(3):292-307.http://dx.doi.org/10.1111/jpi.12264
8. Chen QY, et al.(2019). Metals and Mechanisms of Carcinogenesis. Annual review of pharmacology and toxicology;59:537-54.http://dx.doi.org/10.1146/annurev-pharmtox-010818-021031
9. Sun X, et al.(2021). Amplifying STING activation by cyclic dinucleotide-manganese particles for local and systemic cancer metalloimmunotherapy. Nature nanotechnology;16(11):1260-70.http://dx.doi.org/10.1038/s41565-021-00962-9
10. Chen X, et al.(2021). Cellular degradation systems in ferroptosis. Cell death and differentiation;28(4):1135-48.http://dx.doi.org/10.1038/s41418-020-00728-1
11. Chen X, et al.(2021). Broadening horizons: the role of ferroptosis in cancer. Nature reviews Clinical oncology;18(5):280-96.http://dx.doi.org/10.1038/s41571-020-00462-0
12. Li D, et al.(2020). The interaction between ferroptosis and lipid metabolism in cancer. Signal transduction and targeted therapy;5(1):108.http://dx.doi.org/10.1038/s41392-020-00216-5
13. Blockhuys S, et al.(2017). Defining the human copper proteome and analysis of its expression variation in cancers. Metallomics : integrated biometal science;9(2):112-

23.http://dx.doi.org/10.1039/c6mt00202a
14. Lopez J, et al.(2019). Copper Depletion as a Therapeutic Strategy in Cancer. Metal ions in life sciences;19.http://dx.doi.org/10.1515/9783110527872-018
15. Shanbhag V, et al.(2019). ATP7A delivers copper to the lysyl oxidase family of enzymes and promotes tumorigenesis and metastasis. Proceedings of the National Academy of Sciences of the United States of America;116(14):6836-41.http://dx.doi.org/10.1073/pnas.1817473116
16. Tsang T, et al.(2020). Copper is an essential regulator of the autophagic kinases ULK1/2 to drive lung adenocarcinoma. Nature cell biology;22(4):412-24.http://dx.doi.org/10.1038/s41556-020-0481-4
17. Hwang JJ, et al.(2007). Copper activates TrkB in cortical neurons in a metalloproteinase-dependent manner. Journal of neuroscience research;85(10):2160-6.http://dx.doi.org/10.1002/jnr.21350
18. He F, et al.(2019). Copper (II) Ions Activate Ligand-Independent Receptor Tyrosine Kinase (RTK) Signaling Pathway. BioMed research international;2019:4158415.http://dx.doi.org/10.1155/2019/4158415
19. Opazo CM, et al.(2021). Nutrient copper signaling promotes protein turnover by allosteric activation of ubiquitin E2D conjugases.2021.02.15.431211.http://dx.doi.org/10.1101/2021.02.15.431211 %J bioRxiv
20. Wang Y, et al.(2022). Cuproptosis: a new form of programmed cell death. Cellular & molecular immunology.http://dx.doi.org/10.1038/s41423-022-00866-1
21. Li K, et al.(2021). Advances in clinical immunotherapy for gastric cancer. Biochimica et biophysica acta Reviews on cancer;1876(2):188615.http://dx.doi.org/10.1016/j.bbcan.2021.188615
22. Zeng D, et al.(2021). Tumor microenvironment evaluation promotes precise checkpoint immunotherapy of advanced gastric cancer. Journal for immunotherapy of cancer;9(8).http://dx.doi.org/10.1136/jitc-2021-002467
23. Wang C, et al.(2020). Metalloimmunology: The metal ion-controlled immunity. Advances in immunology;145:187-241.http://dx.doi.org/10.1016/bs.ai.2019.11.007
24. Voli F, et al.(2020). Intratumoral Copper Modulates PD-L1 Expression and Influences Tumor Immune Evasion. Cancer research;80(19):4129-44.http://dx.doi.org/10.1158/0008-5472.Can-20-0471
25. Hu Frisk JM, et al.(2017). Copper Regulates Maturation and Expression of an MITF:Tryptase Axis in Mast Cells. Journal of immunology (Baltimore, Md : 1950);199(12):4132-41.http://dx.doi.org/10.4049/jimmunol.1700786
26. Pan Y, et al.(2020). Tumor-Associated Macrophages in Tumor Immunity. Frontiers in immunology;11:583084.http://dx.doi.org/10.3389/fimmu.2020.583084
27. Li W, et al.(2019). Gastric cancer-derived mesenchymal stromal cells trigger M2 macrophage polarization that promotes metastasis and EMT in gastric cancer. Cell death & disease;10(12):918.http://dx.doi.org/10.1038/s41419-019-2131-y
28. Viitala M, et al.(2019). Immunotherapeutic Blockade of Macrophage Clever-1 Reactivates the CD8(+) T-cell Response against Immunosuppressive Tumors. Clinical cancer research : an official journal of

the American Association for Cancer Research;25(11):3289-303.http://dx.doi.org/10.1158/1078-0432.Ccr-18-3016

29. Junttila A, et al.(2020). Immunophenotype based on inflammatory cells, PD-1/PD-L1 signalling pathway and M2 macrophages predicts survival in gastric cancer. British journal of cancer;123(11):1625-32.http://dx.doi.org/10.1038/s41416-020-01053-7
30. Bonneville R, et al.(2017). Landscape of Microsatellite Instability Across 39 Cancer Types. JCO precision oncology;2017.http://dx.doi.org/10.1200/po.17.00073
31. Shitara K, et al.(2020). Efficacy and Safety of Pembrolizumab or Pembrolizumab Plus Chemotherapy vs Chemotherapy Alone for Patients With First-line, Advanced Gastric Cancer: The KEYNOTE-062 Phase 3 Randomized Clinical Trial. JAMA oncology;6(10):1571-80.http://dx.doi.org/10.1001/jamaoncol.2020.3370
32. Shitara K, et al.(2018). Pembrolizumab versus paclitaxel for previously treated, advanced gastric or gastro-oesophageal junction cancer (KEYNOTE-061): a randomised, open-label, controlled, phase 3 trial. Lancet (London, England);392(10142):123-33.http://dx.doi.org/10.1016/s0140-6736(18)31257-1
33. Chowell D, et al.(2018). Patient HLA class I genotype influences cancer response to checkpoint blockade immunotherapy. Science (New York, NY);359(6375):582-7.http://dx.doi.org/10.1126/science.aao4572

Figures

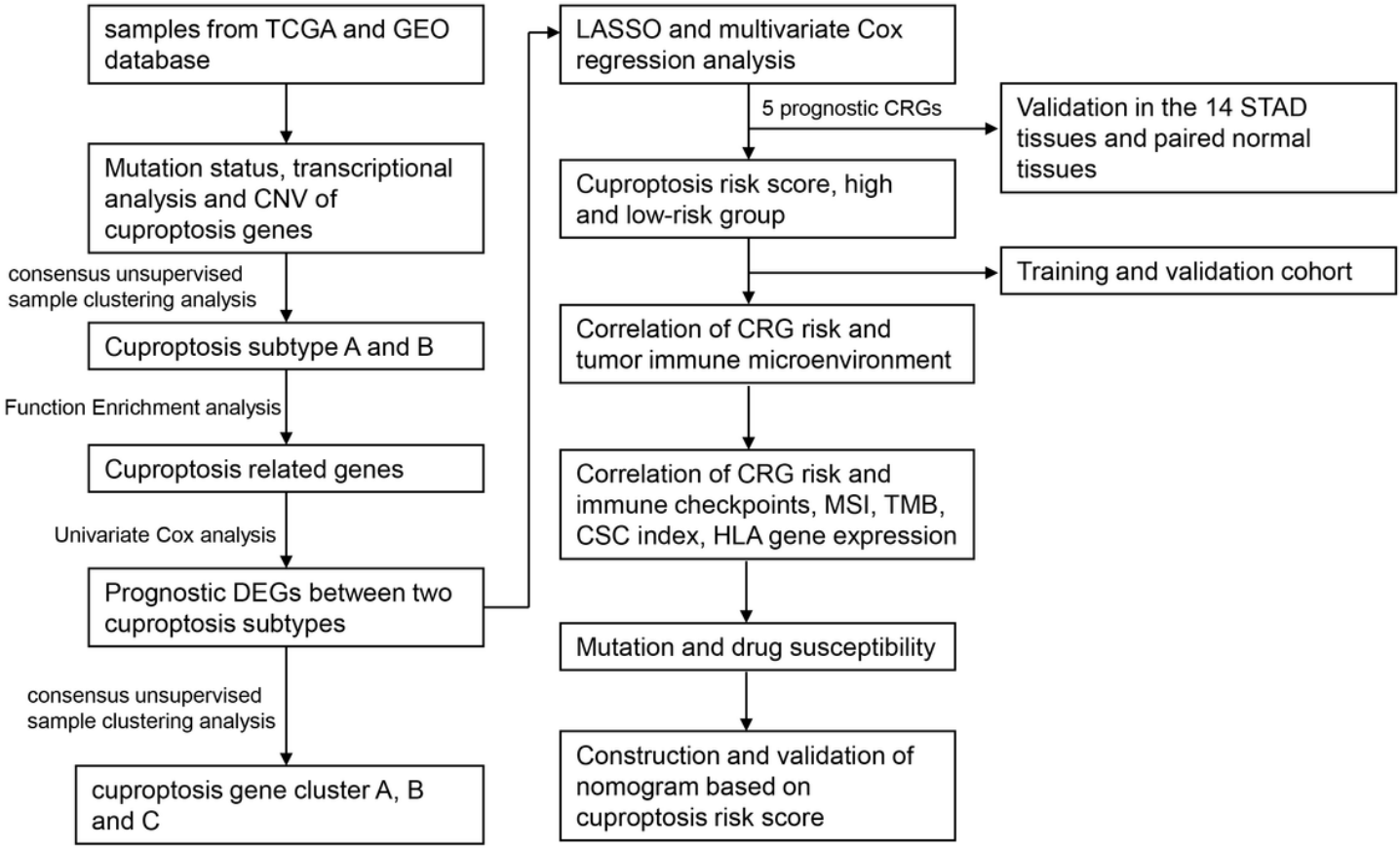

Figure 1

Flowchart of the present study.

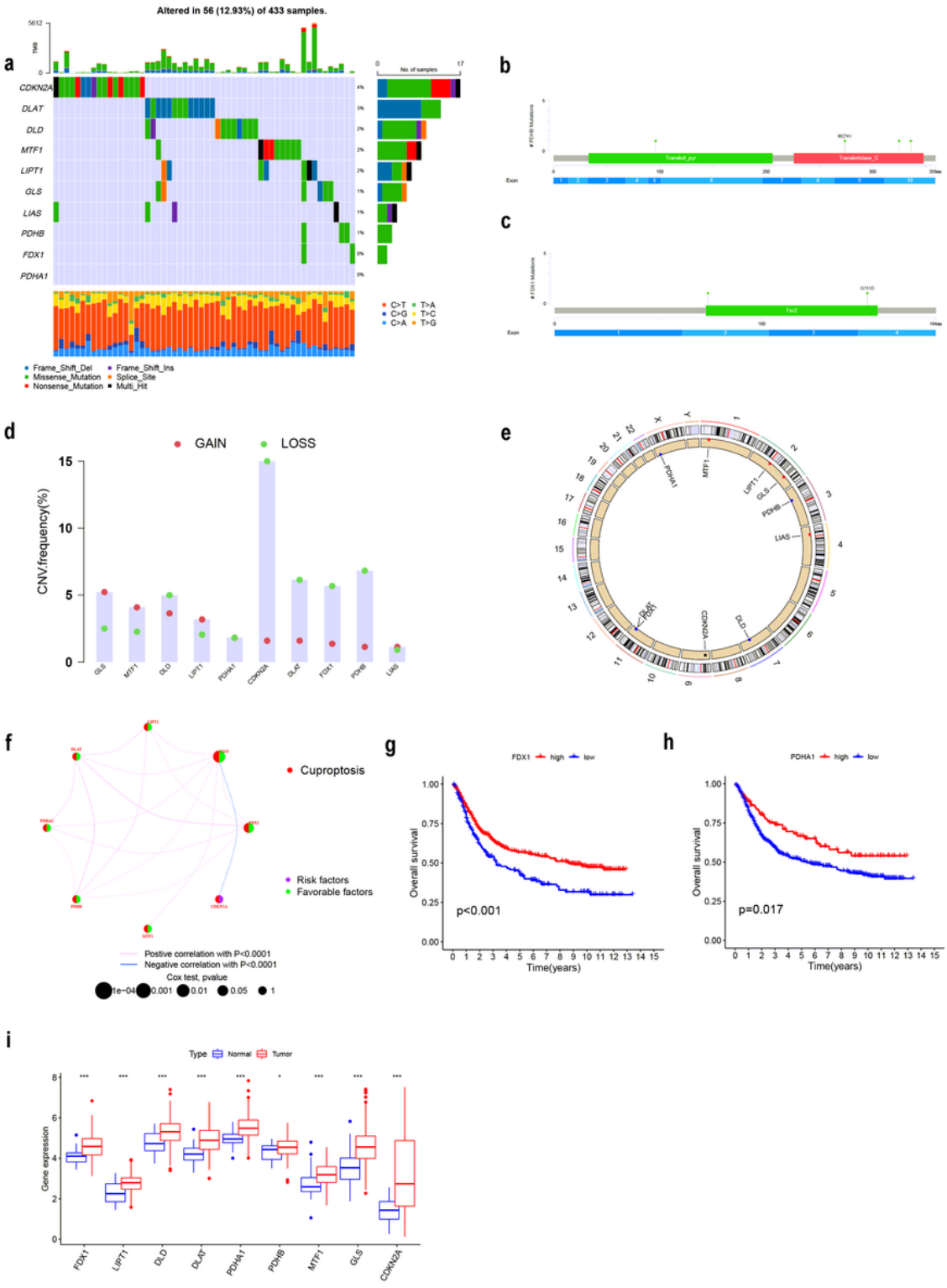

Figure 2

Genetic and transcriptional analysis of cuproptosis genes in STAD. (a) Mutation frequencies of 10 cuproptosis genes in STAD patients from TCGA. (b.c) Mutational analysis of *PDHB* and *FDX1* according to the Cbioportal database. (d) Copy number variation of CRGs. (e) Locations of CRGs CNV on 23 chromosomes. (f) Interactions among CRGs in STAD. The line connecting the CRGs represents their interaction. Blue represents negative and pink represents positive correlations, respectively. (g.h) Kaplan-

Meier analysis based on the expression of *FDX1* and *PAHA1*. (i) Expression differences of CRGs between normal and STAD samples.

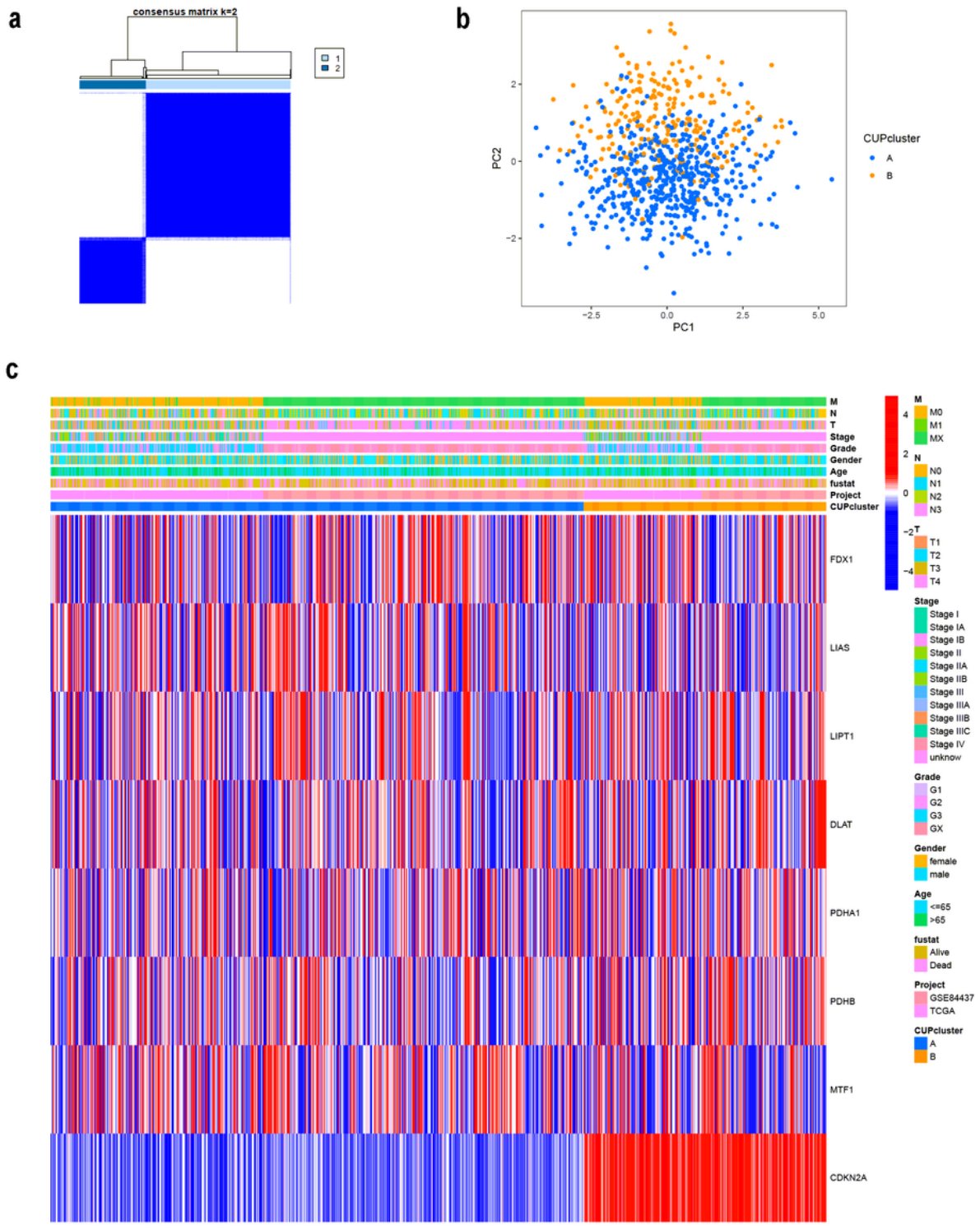

Figure 3

Cuproptosis subtypes in STAD. (a) Consensus matrix heatmap identifying 2 clusters (k=2). (b) PCA analysis showing a significant difference in cuproptosis transcription profile. (c) Differences in clinicopathological factors and CRGs expression between two cuproptosis clusters.

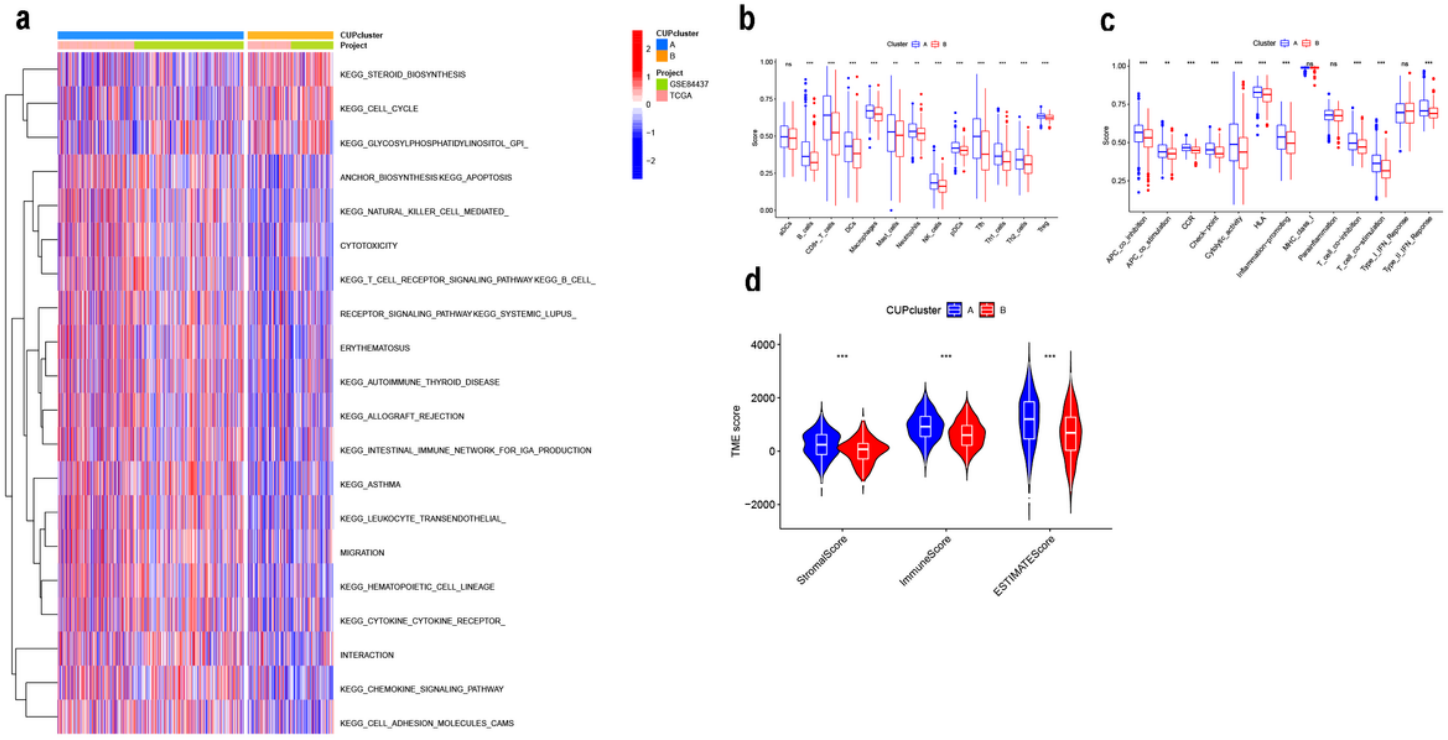

Figure 4

(a) GSVA analysis of the biological pathways between cuproptosis subtypes. (b) Immune cells infiltrate between different cuproptosis clusters. (c) Immune functions between different cuproptosis clusters. (d) Correlation of cuproptosis clusters with immune/stromal scores.

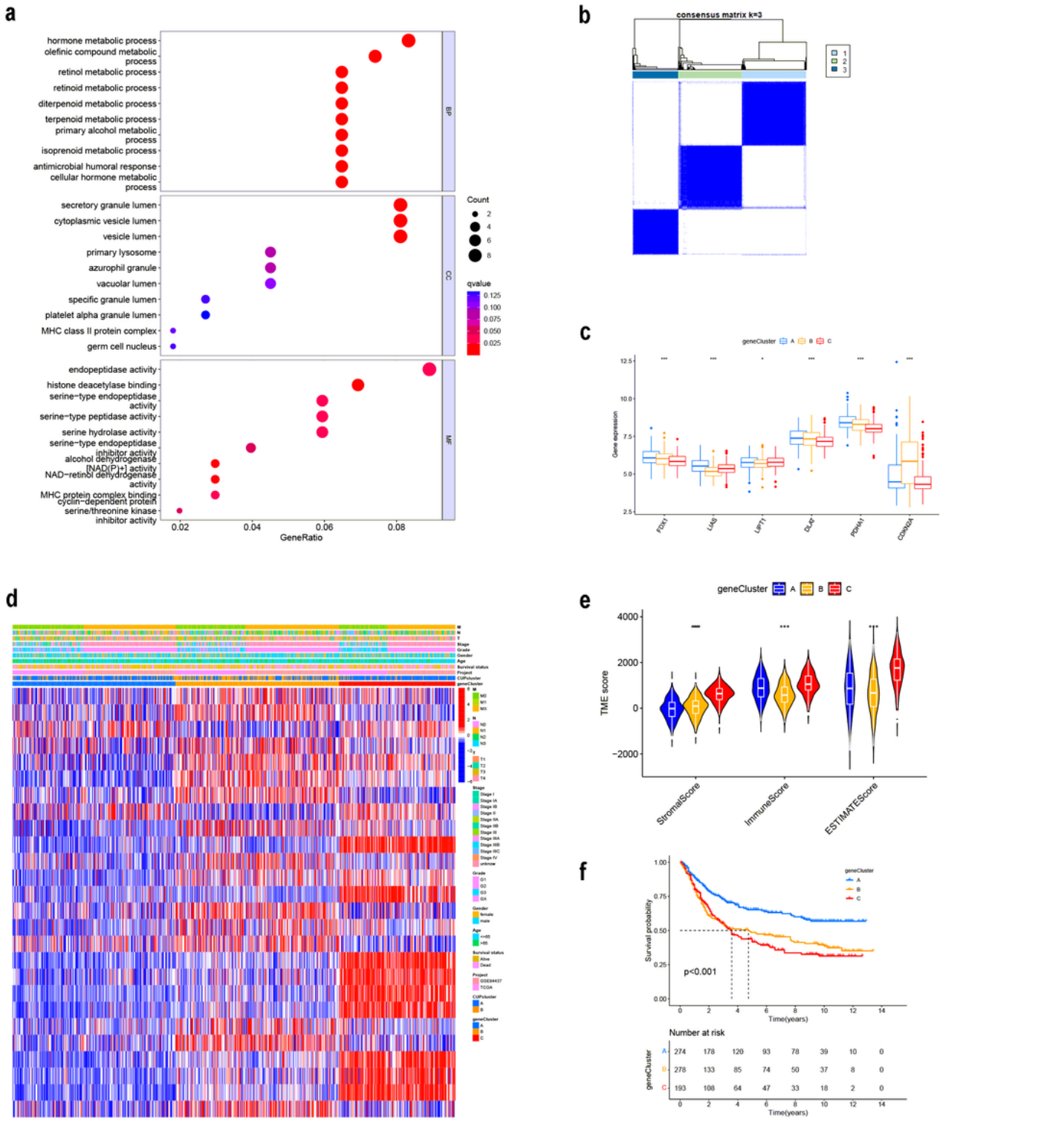

Figure 5

(a) GO analysis of DEGs between two cuproptosis subtypes. (b) Consensus matrix heatmap identifying 3 clusters (k=3). (c) Differences in CRG expression between three gene clusters. (d) Differences in clinicopathological factors and CRGs expression between three gene clusters. (e) Correlation of gene clusters with immune/stromal scores. (f) Survival analysis showing gene clusters were associated with OS in STAD patients.

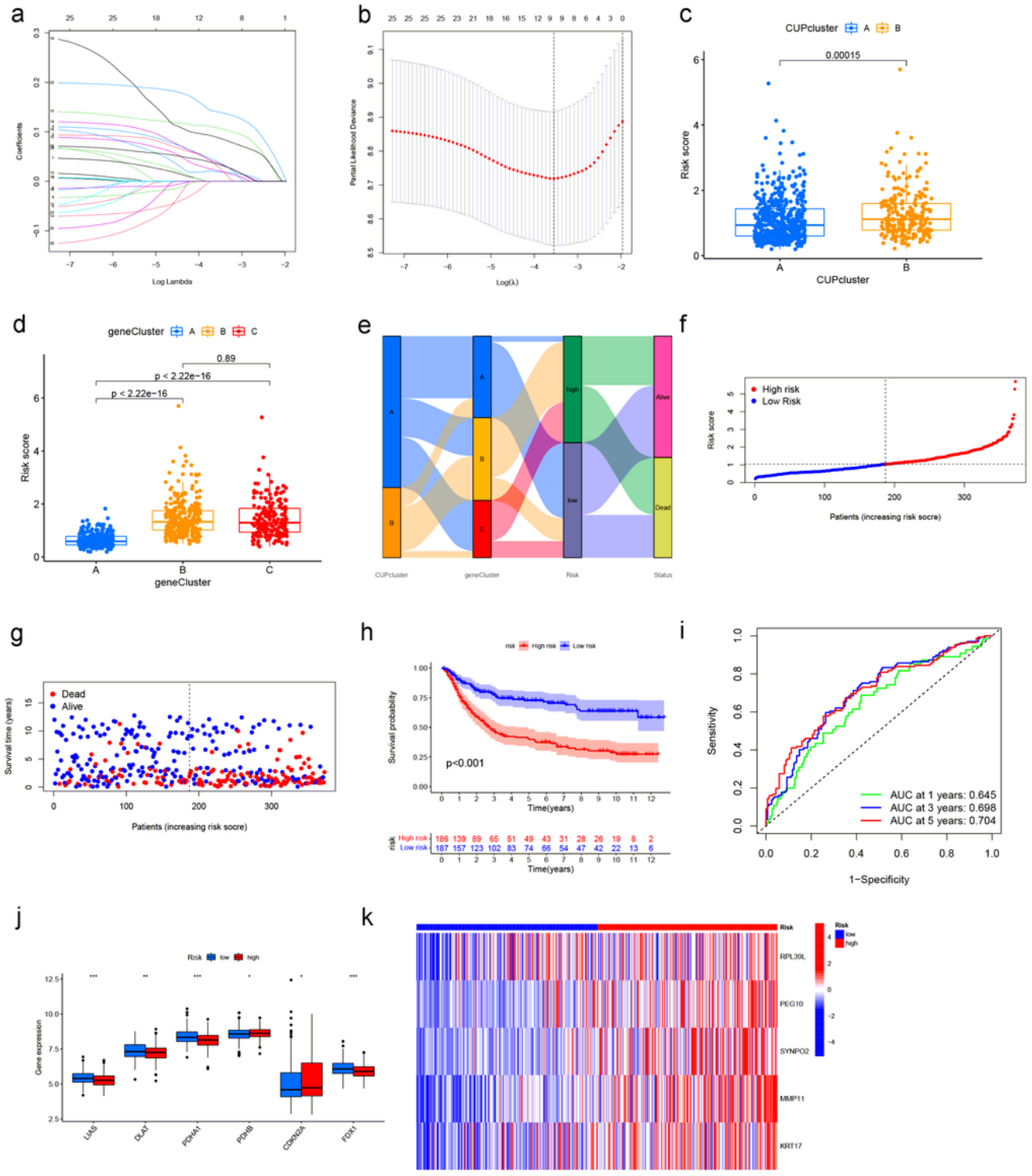

Figure 6

Construction of the cuproptosis gene risk score for STAD patients. (a, b) LASSO regression analysis and partial likelihood deviance of the prognostic genes. (c, d) CRG risk score distribution in different cuproptosis and gene clusters. (e) Correlation of cuproptosis subtype, gene subtype, CRG risk score, and survival outcomes. (f-g) Ranked dot and scatter plot showing the CRG risk score and survival status in the training cohort. (h) Survival analysis of the OS between the high and low-risk groups. (i) ROC analysis of

the predictive ability of OS at 1, 3, 5, and 10 years according to the CRG risk score. (j) Cuproptosis genes differentially expressed between high and low-risk groups. (k) The 5 prognostic CRGs in the model between high and low-risk groups.

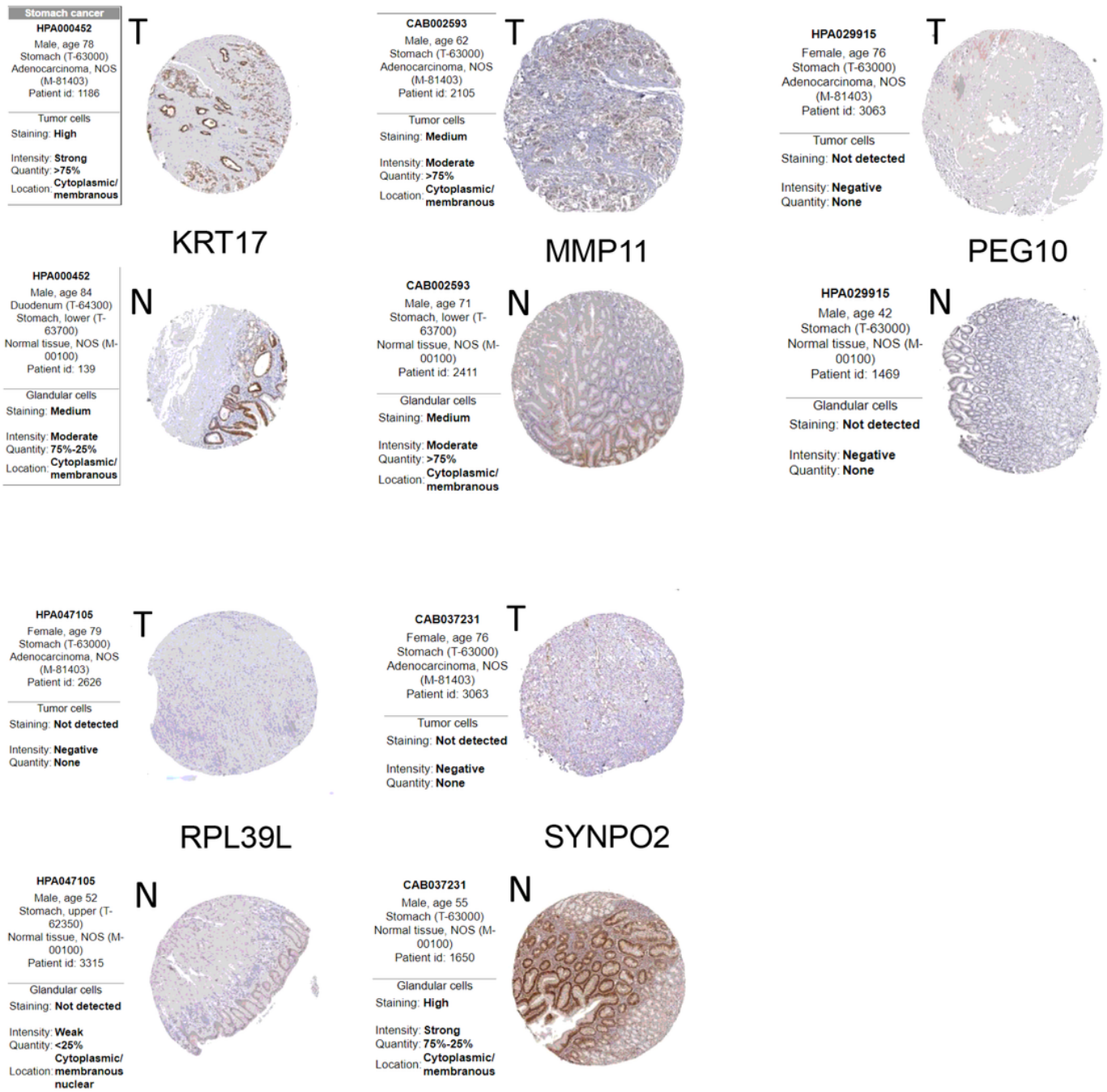

Figure 7

Validation of the protein expression in the cuproptosis risk model on the HPA website.

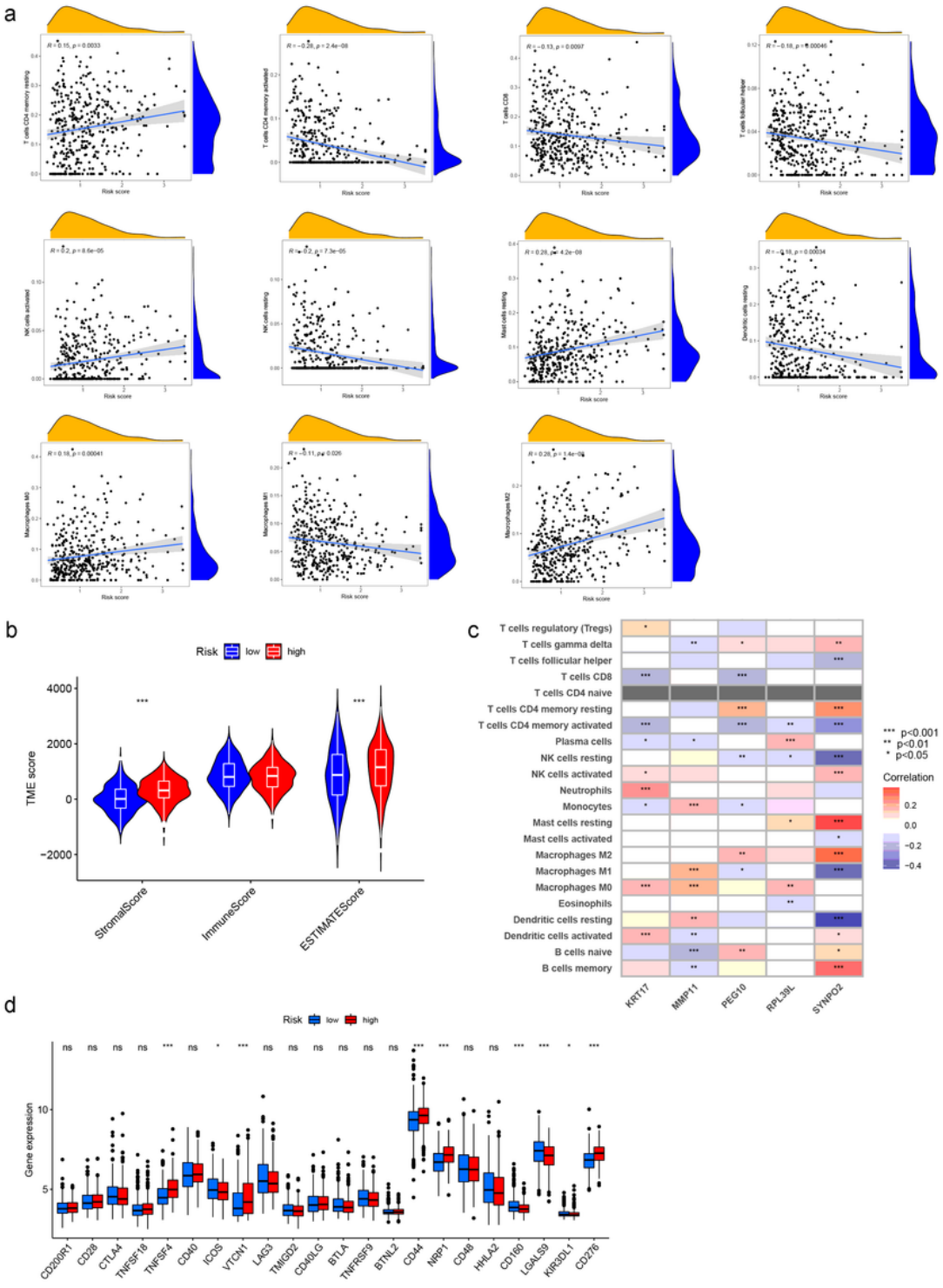

Figure 8

Association of TIME with the cuproptosis risk score. (a) Correlation of infiltrating immune cells with a CRG risk score. (b) Correlation of CRG risk_score with immune/stromal scores. (c) Correlation of immune cells with 5 CRGs. (d) Correlation between the CRG risk score and immune checkpoint gene expression.

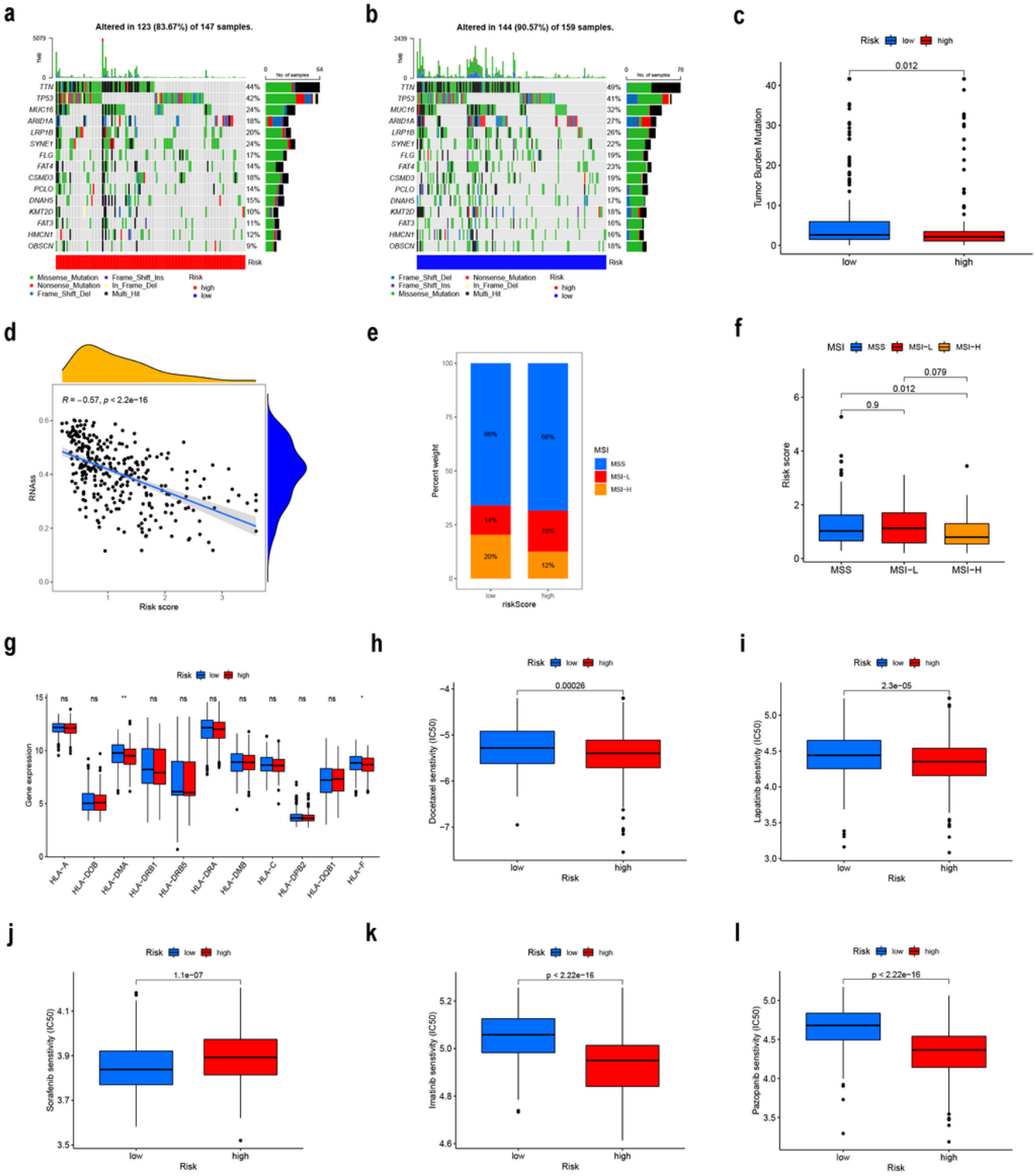

Figure 9

Comprehensive analysis of cuproptosis risk score in STAD. (a,b) Somatic mutation features in the high- and low-risk groups. (c) Correlation of CRG risk_score and TMB. (d) Correlation of CRG risk_score and CSC index. (e,f) Correlation of CRG risk_score and MSI status. (g) Correlation of CRG risk_score and HLA gene expression. (h-l) Drug susceptibility analysis of chemotherapy and targeted therapy in high- and low-risk groups.

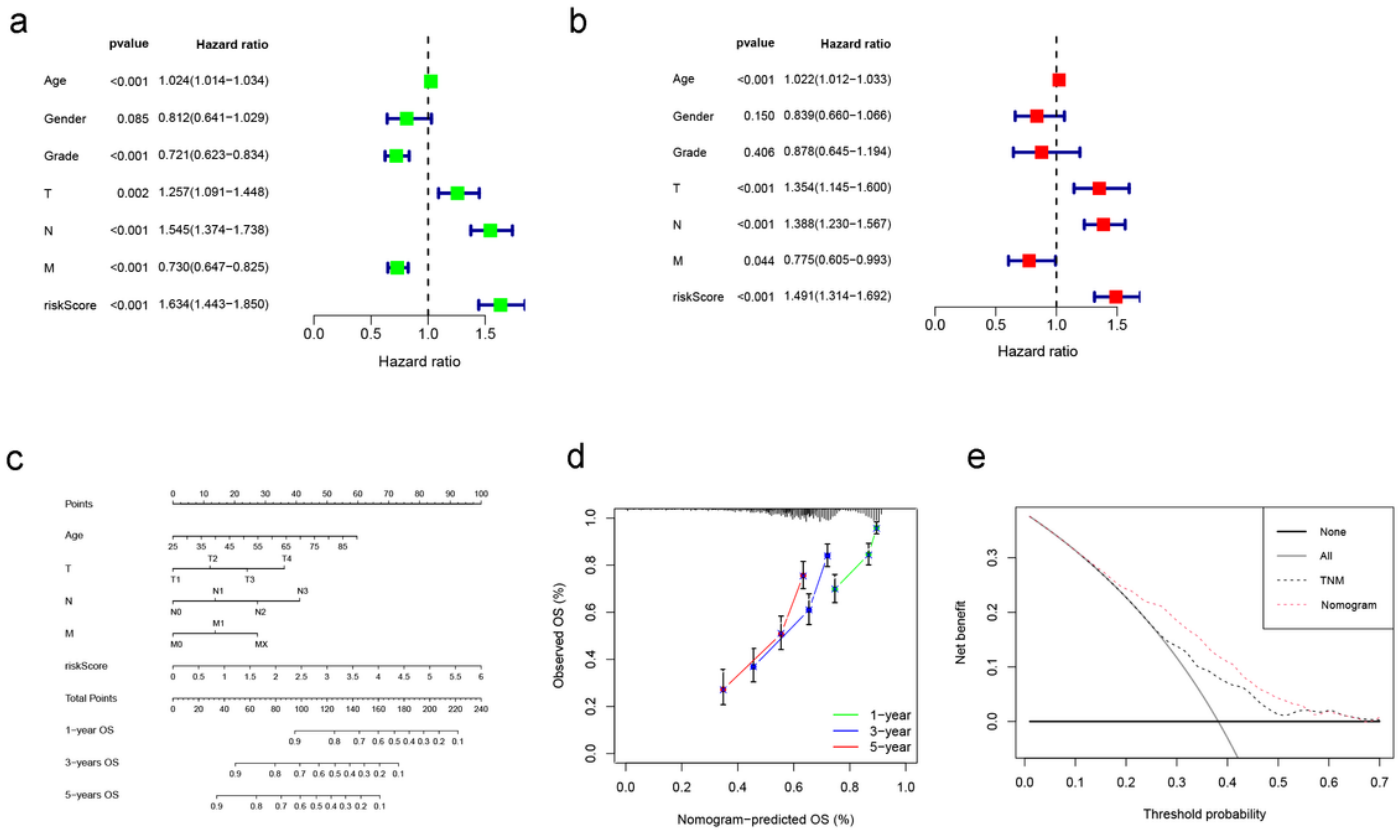

Figure 10

Construction and validation of the nomogram based on the cuproptosis risk score. (a-b) Univariate and multivariate Cox analysis of prognostic factors. (c) Nomogram predicting the 1-, 3-, and 5-year OS in STAD patients. (d) Calibration curve for prediction of 1-,3- and 5-year OS in STAD patients. (e) Decision curve analyses of the nomogram.

Supplementary Files

This is a list of supplementary files associated with this preprint. Click to download.

- SupplementaryFigures.docx
- SupplentaryTables.xlsx